

Phase Relations in the BaO–Al₂O₃–AlN System: Materials with the β -Alumina Structure

S. R. Jansen,¹ H. T. Hintzen, and R. Metselaar

Centre for Technical Ceramics, Laboratory of Solid State Chemistry and Materials Science, Eindhoven University of Technology, P.O. Box 513, 5600 MB Eindhoven, The Netherlands

Received March 21, 1996; in revised form November 12, 1996; accepted November 18, 1996

It is generally known that aluminates with the β -alumina-type structure exhibit very useful optical and electrical properties. In this paper the synthesis of a new compound, namely barium aluminium-oxynitride with the β -alumina structure (space group $P6_3/mmc$) is reported. To obtain additional information, the BaO–Al₂O₃–AlN phase diagram was investigated at 1400, 1500, 1650, and 1700°C. The ideal composition of this new material is BaAl₁₁O₁₆N. The unit cell dimensions of the material with the ideal composition (after firing at 1700°C) are $a = 5.6019$ (2) Å and $c = 22.6579$ (8) Å, so $c/a = 4.0447$ (2). We determined a solid solution between the already known barium β -alumina (or barium hexaaluminate phase I) with the composition BaAl_{13.8}O_{21.7} and the new barium aluminium-oxynitride. The extent of this solid solution is dependent on the firing temperature. For this solid solution the c axis is decreasing, while the a axis is increasing with increasing nitrogen content. © 1997

Academic Press

INTRODUCTION

Aluminates with the β -alumina- or the magnetoplumbite-type structure show interesting optical and electrical properties (1–3). These two structures are related, built up of spinel blocks and intermediate layers, allowing various substitutions (1, 4, 5).

Starting from the compound SrAl₁₂O₁₉, a material with the magnetoplumbite-type structure, it is possible to replace Sr²⁺ by La³⁺ when simultaneously Al³⁺ is substituted by Mg²⁺ for charge compensation. This results in the compound LaMgAl₁₁O₁₉ that is used in fluorescent lamps after substitution of La³⁺ by Ce³⁺ and Tb³⁺ (6). Recently, a new type of charge compensation was reported, namely replacing O²⁻ by N³⁻ instead of Al³⁺ by Mg²⁺. This results in the compound LaAl₁₂O₁₈N (7–10).

Materials with the composition NaAl₁₁O₁₇ having the β -alumina-type structure show very good ionic conductivity

¹ To whom correspondence should be addressed. E-mail: tgtvsj@chem.tue.nl.

(5, 11, 12). An interesting observation is that the ionic conductivity can be increased by introducing N³⁻ ions (13). Another compound can be derived from NaAl₁₁O₁₇, in a similar way as done for SrAl₁₂O₁₉: by substitution of Na⁺ by Ba²⁺ and simultaneously replacing Al³⁺ by Mg²⁺ to obtain charge compensation. This results in BaMgAl₁₁O₁₇, which shows a very efficient blue luminescence after Eu²⁺ doping on the Ba²⁺ site and for this reason the material is currently used in fluorescent lamps (3, 14, 15). Because of the similarity with the magnetoplumbite-type structure, we envisaged that the replacement of O²⁻ by N³⁻ might also be possible in the β -alumina-type structure, resulting in the ideal composition BaAl₁₁O₁₆N. The existence of such a compound was recently proven by us and the reactivity of various starting materials was investigated to synthesize this material. These results have been published elsewhere (16).

This paper presents the results of the investigation of the phase diagram of the BaO–Al₂O₃–AlN system. In the BaO–Al₂O₃ part of this system, two types of barium hexaaluminates exist (17, 18): barium hexaaluminate phase I (BaAl_{13.8}O_{21.7}) with the β -alumina-type structure and barium hexaaluminate phase II (BaAl_{9.2}O_{14.8}) with a β' -alumina-like structure. Due to intergrowth of these phases, their exact compositions are unknown (19–21). A solid solution between barium hexaaluminate phase I (BaAl_{13.8}O_{21.7}) and BaAl₁₁O₁₆N appears to exist, but its extent is dependent on firing temperature. Preliminary results of this study have been published elsewhere (22).

EXPERIMENTAL PROCEDURES

To obtain a good overview of the phase diagram, in total 40 compositions were prepared. The starting mixtures were made by combining the appropriate amounts of BaCO₃ (Merck, > 99.0%), γ -Al₂O₃ (AKPG, > 99.995%), and AlN (Starck grade C, > 97%). Corrections were made for weight losses and for the oxygen content of AlN. The choice of the Al₂O₃-type raw material is based on our previous study (16). The powder was wet-mixed in isopropanol (> 99.7%)

for 2 hr in an agate container with agate balls. A planetary ball mill was used for the mixing. After mixing, the isopropanol was evaporated. The powder was dried in a stove for one night at 160°C and it was subsequently ground in an agate mortar.

Reactions were performed in a vertical high-temperature tube furnace at four different temperatures: 1400°C (10 hr), 1500°C (5 hr), 1650°C (2 hr), and 1700°C (2 hr). At 1700°C, only those compositions which are on the solid solution line were examined. The reaction times were chosen in such a way that an equilibrium situation was reached. This was checked by repeated firing. For those samples with the same composition as AlON (72 to 80% Al₂O₃ and 28 to 20% AlN) the firing time at 1650°C was 40 hr (equal to the conditions used by Willems (23)). In all cases a N₂/H₂ gas flow was used and the powder mixtures were fired in molybdenum crucibles.

The phases, present after reaction, were determined by powder X-ray diffraction (XRD). Continuous scans were made with CuK α radiation from 5° to 75° (2 θ), with a scan speed of 1° (2 θ)/min (Philips 5100). Step scans, with a step size of 0.01° (2 θ) and a counting time of 6 s/step, were made from 68° to 75° (2 θ) in order to determine the presence of traces of AlN. For careful determination of the unit cell dimensions of the single phase materials, step scans were used with Si as internal standard. Again, CuK α radiation (Philips 5100 or Rigaku) was used, in the region from 5° to 105° (2 θ), with a step size of 0.01° (2 θ) and a counting time of 6 s/step. The following reflections are used for the calculation of the unit cell dimensions: 3 0 4, 1 0 14, 1 0 15, 2 1 10, 2 0 13, 2 2 0, 2 0 14, 1 1 16, 3 1 7, 2 0 17, 0 0 20, and 2 2 14.

RESULTS

A typical XRD pattern of the new oxynitride BaAl₁₁O₁₆N is depicted in Fig. 1. The incorporation of N³⁻ in this structure is concluded from a shift of the reflections in the XRD pattern caused by a change of the unit cell dimensions. The crystallographic data and reflec-

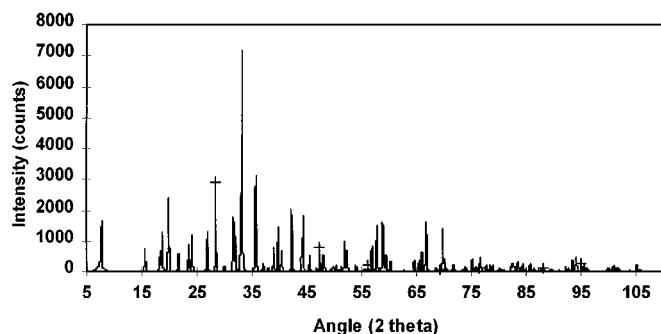


FIG. 1. A typical X-ray diffraction pattern of BaAl₁₁O₁₆N, which is fired at 1700°C. Peaks of the internal standard (Si) are marked with +.

TABLE 1
Crystallographic Data of BaAl_{13.8}O_{21.7} and BaAl₁₁O₁₆N,
Which Were Formed after Firing at 1700°C

Radiation: CuK α_1	Wavelength: 1.5406 Å	Filter: Ni
BaAl _{13.8} O _{21.7} (barium hexaaluminate phase I)		
System: hexagonal	Space group: <i>P6₃/mmc</i> (194)	
Unit cell	$a = 5.5873 (\pm 0.0003) \text{ \AA}$	$c = 22.7207 (\pm 0.0012) \text{ \AA}$
$c/a = 4.066$	$V = 614.25 (\pm 0.07) \text{ \AA}^3$	Molar mass = 856.85 g/mol
Color: white		
BaAl ₁₁ O ₁₆ N		
System: hexagonal	Space group: <i>P6₃/mmc</i> (194)	
Unit cell	$a = 5.6019 (\pm 0.0002) \text{ \AA}$	$c = 22.6579 (\pm 0.0008) \text{ \AA}$
$c/a = 4.045$	$V = 615.78 (\pm 0.05) \text{ \AA}^3$	Molar mass = 733.65 g/mol
Color: white		

tions of BaAl_{13.8}O_{21.7} and BaAl₁₁O₁₆N, prepared at 1700°C, are shown in Tables 1 to 3. The phase diagram at 1650°C is shown in Fig. 2. As is clear from this figure, at 1650°C a solid solution exists between barium hexaaluminate phase I and the N³⁻ substituted compound. The phase diagrams at 1400 and 1500°C are similar; only the extent of the solid solution line decreases with decreasing temperature. As a consequence of the N³⁻ incorporation, XRD peak shifts and peak intensities change. However no systematic relationship is found between the peak intensities and the composition of the β -alumina structure. Figures 3 to 5 show the a axis, the c axis, and the c/a ratio, respectively, as a function of the sample composition (represented by x in the general formula BaAl_{13.8-2.8x}O_{21.7-5.7x}N_x, on the solid solution line) and of the firing temperature (1400, 1500, 1650, and 1700°C). The standard deviations of the calculated cell parameters are also depicted in these figures.

DISCUSSION

The incorporation of N³⁻ in barium hexaaluminate phase I is proved in several ways:

1. the phase diagram, as presented in Fig. 2, does not show secondary phases for the N containing mixtures, which only can be explained by the incorporation of nitrogen;
2. the unit cell dimensions of the material on the line BaAl_{13.8-2.8x}O_{21.7-5.7x}N_x depends on the amount of AlN in the starting mixture;
3. neutron diffraction measurements on BaAl₁₁O₁₆N clearly indicate the preferential incorporation of N³⁻ on two distinct sites (24).

The first two points will be discussed in more detail in the following paragraphs.

With an increasing amount of AlN in the starting mixture changes are observed in the unit cell dimensions of reacted

TABLE 2
Reflections Attributed to Barium Hexaaluminate Phase I ($\text{BaAl}_{13.8}\text{O}_{21.7}$), Which Was Formed after Firing at 1700°C

d_{measured} Å	$d_{\text{calculated}}$ Å	I/I_{max} %	h	k	l	d_{measured} Å	$d_{\text{calculated}}$ Å	I/I_{max} %	h	k	l
11.34	11.36	66	0	0	2	1.3692	1.3693	2	2	1	11
5.67	5.68	25	0	0	4	1.3477	1.3478	27	2	0	14
4.83	4.84	4	1	0	0	1.3326	1.3327	1	3	1	2
4.73	4.73	9	1	0	1	1.3154	1.3154	2	2	1	12
4.45	4.45	23	1	0	2	1.3058	1.3061	1	3	1	4
4.077	4.078	4	1	0	3	1.2878	1.2871	1	3	1	5
3.784	3.787	7	0	0	6	1.2839	1.2838	2	2	0	15
3.682	3.683	12	1	0	4	1.2660	1.2659	7	1	1	16
3.311	3.312	12	1	0	5	1.2533	1.2534	2	2	2	8
2.9819	2.9821	1	1	0	6	1.2403	1.2402	6	3	1	7
2.8386	2.8401	32	0	0	8	1.2279	1.2278	2	3	0	12
2.7928	2.7936	17	1	1	0	1.2215	1.2214	4	1	0	18
2.6946	2.6955	100	1	0	7	1.2139	1.2139	2	2	1	14
2.5062	2.5068	35	1	1	4	1.2099	1.2097	< 1	4	0	0
2.4188	2.4194	3	2	0	0	1.1947	1.1945	1	4	0	3
2.3672	2.3663	1	2	0	2	1.1901	1.1899	1	2	2	10
2.3042	2.3046	7	2	0	3	1.1696	1.1699	4	2	0	17
2.2713	2.2721	34	0	0	10	1.1665	1.1666	3	2	1	15
2.2256	2.2259	8	2	0	4	1.1609	1.1609	4	1	0	19
2.1354	2.1355	28	2	0	5	1.1557	1.1555	1	3	1	10
2.0563	2.0566	16	1	0	10	1.1526	1.1523	2	4	0	6
2.0387	2.0388	24	2	0	6	1.1503	1.1503	4	1	1	18
1.9920	1.9916	6	1	1	8	1.1439	1.1440	< 1	3	0	14
1.9396	1.9398	2	2	0	7	1.1361	1.1360	6	0	0	20
1.8995	1.8997	8	1	0	11	1.1331	1.1335	< 1	4	0	7
1.8939	1.8934	8	0	0	12	1.1248	1.1253	1	3	1	11
1.8414	1.8417	2	2	0	8	1.1191	1.1191	1	2	0	18
1.8286	1.8289	1	2	1	0	1.1058	1.1060	1	1	0	20
1.8228	1.8230	1	2	1	1	1.0949	1.0949	< 1	3	1	12
1.8055	1.8056	2	2	1	2	1.0911	1.0909	1	4	0	9
1.7773	1.7778	2	2	1	3	1.0783	1.0784	< 1	3	2	5
1.7629	1.7632	12	1	0	12	1.0721	1.0720	3	2	0	19
1.7466	1.7467	8	2	0	9	1.0659	1.0658	2	3	0	16
1.7411	1.7408	3	2	1	4	1.0587	1.0587	4	2	2	14
1.6962	1.6966	2	2	1	5	1.0559	1.0559	7	4	1	0
1.6561	1.6562	1	2	0	10	1.0528	1.0523	1	1	1	20
1.6228	1.6229	17	0	0	14	1.0503	1.0503	2	3	2	7
1.6126	1.6129	2	3	0	0	1.0437	1.0438	2	4	0	11
1.5932	1.5933	18	2	1	7	1.0385	1.0388	3	2	1	18
1.5707	1.5709	24	2	0	11	1.0342	1.0342	1	3	1	14
1.5665	1.5673	12	1	1	12	1.0171	1.0171	< 1	4	1	6
1.5515	1.5516	5	3	0	4	1.0101	1.0100	2	1	0	22
1.5388	1.5387	6	1	0	14	1.0043	1.0045	1	3	1	15
1.4838	1.4839	< 1	3	0	6	1.0010	1.0009	3	2	1	19
1.4456	1.4455	6	1	0	15	0.9946	0.9947	3	4	0	13
1.4245	1.4247	5	2	1	10	0.9875	0.9877	< 1	2	0	21
1.4169	1.4167	15	2	0	13	0.9780	0.9778	< 1	3	2	11
1.4031	1.4033	4	1	1	14	0.9700	0.9699	4	4	0	14
1.3968	1.3968	20	2	2	0	0.9684	0.9687	1	1	1	22

Note. The crystallographic data are shown in Table 1. d_{measured} is corrected for the internal standard (Si).

TABLE 3
Reflections Attributed to BaAl₁₁O₁₆N₃, Which Was Formed after Firing at 1700°C

d_{measured} Å	$d_{\text{calculated}}$ Å	I/I_{max} %	h	k	l	d_{measured} Å	$d_{\text{calculated}}$ Å	I/I_{max} %	h	k	l
11.41	11.33	23	0	0	2	1.3361	1.3361	1	3	1	2
5.67	5.66	10	0	0	4	1.3241	1.3247	< 1	3	1	3
4.86	4.85	7	1	0	0	1.3160	1.3163	3	3	0	10
4.75	4.74	18	1	0	1	1.3093	1.3091	1	3	1	4
4.467	4.460	33	1	0	2	1.2898	1.2899	1	3	1	5
4.088	4.082	8	1	0	3	1.2823	1.2822	2	2	0	15
3.778	3.776	12	0	0	6	1.2637	1.2638	6	1	1	16
3.689	3.685	17	1	0	4	1.2554	1.2554	2	2	2	8
3.314	3.312	18	1	0	5	1.2424	1.2425	6	3	1	7
2.9797	2.9799	2	1	0	6	1.2281	1.2282	3	3	0	12
2.8329	2.8322	25	0	0	8	1.2230	1.2230	1	2	0	16
2.8018	2.8010	22	1	1	0	1.2184	1.2184	3	1	0	18
2.7188	2.7191	11	1	1	2	1.2133	1.2134	3	2	1	14
2.6934	2.6926	100	1	0	7	1.1975	1.1975	1	4	0	3
2.5110	2.5108	43	1	1	4	1.1916	1.1913	1	2	2	10
2.4474	2.4459	< 1	1	0	8	1.1876	1.1867	< 1	3	1	9
2.4257	2.4257	4	2	0	0	1.1717	1.1716	2	4	0	5
2.3702	2.3719	1	2	0	2	1.1682	1.1681	4	2	0	17
2.3098	2.3095	11	2	0	3	1.1657	1.1659	2	2	1	15
2.2657	2.2658	20	0	0	10	1.1579	1.1580	4	1	0	19
2.2307	2.2298	9	2	0	4	1.1546	1.1548	2	4	0	6
2.1391	2.1386	29	2	0	5	1.1481	1.1482	3	1	1	18
2.0530	2.0529	15	1	0	10	1.1442	1.1439	1	3	0	14
2.0411	2.0409	26	2	0	6	1.1329	1.1329	3	0	0	20
1.9917	1.9915	7	1	1	8	1.1266	1.1265	1	3	1	11
1.9413	1.9411	1	2	0	7	1.1250	1.1248	1	2	2	12
1.8958	1.8960	7	1	0	11	1.1174	1.1173	< 1	2	0	18
1.8888	1.8882	4	0	0	12	1.1117	1.1116	1	3	2	1
1.8428	1.8424	1	2	0	8	1.1031	1.1032	< 1	1	0	20
1.8334	1.8337	2	2	1	0	1.0959	1.0958	< 1	3	1	12
1.8279	1.8277	2	2	1	1	1.0926	1.0927	1	4	0	9
1.8099	1.8101	3	2	1	2	1.0811	1.0809	< 1	3	2	5
1.7815	1.7819	2	2	1	3	1.0780	1.0781	< 1	2	1	17
1.7610	1.7616	14	1	0	10	1.0702	1.0702	2	2	0	19
1.7463	1.7468	9	2	0	9	1.0655	1.0654	2	3	0	16
1.7000	1.6998	3	2	1	5	1.0591	1.0590	5	2	2	14
1.6552	1.6558	1	2	0	10	1.0531	1.0532	7	1	0	21
1.6498	1.6495	< 1	2	1	6	1.0502	1.0502	1	1	1	20
1.6180	1.6184	12	0	0	14	1.0409	1.0406	3	4	1	4
1.5955	1.5954	21	2	1	7	1.0349	1.0347	1	3	1	14
1.5699	1.5701	23	2	0	11	1.0299	1.0299	< 1	0	0	22
1.5656	1.5656	14	1	1	12	1.0181	1.0179	< 1	3	2	9
1.5548	1.5550	8	3	0	4	1.0077	1.0075	2	1	0	22
1.5351	1.5352	5	1	0	14	1.0050	1.0047	1	3	1	15
1.4826	1.4822	< 1	2	1	9	0.9998	0.9997	3	2	1	19
1.4422	1.4422	5	1	0	15	0.9957	0.9958	1	2	2	16
1.4255	1.4254	5	2	1	10	0.9935	0.9933	1	3	0	18
1.4153	1.4154	9	2	0	13	0.9860	0.9858	< 1	2	0	21
1.4005	1.4005	23	2	2	0	0.9792	0.9792	< 1	3	2	11
1.3695	1.3696	2	2	1	11	0.9708	0.9706	3	4	0	14
1.3462	1.3463	20	2	0	14	0.9668	0.9703	1	5	0	0

Note. The crystallographic data are shown in Table 1. d_{measured} is corrected for the internal standard (Si).

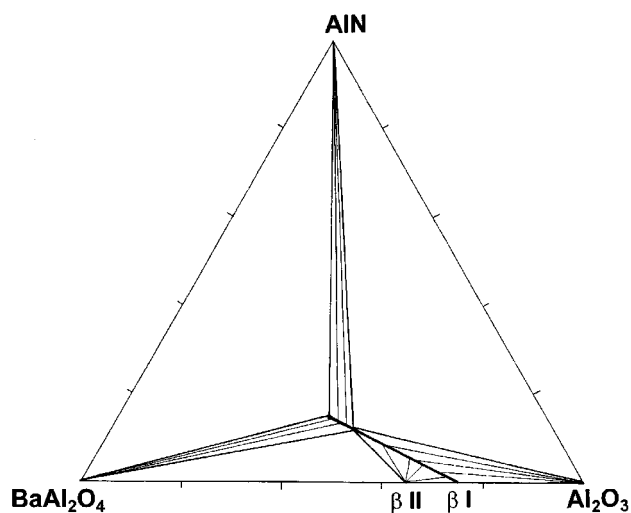


FIG. 2. The phase diagram of the $\text{BaAl}_2\text{O}_4\text{-Al}_2\text{O}_3\text{-AlN}$ system after firing at 1650°C .

single phase barium hexaaluminate phase I. These changes are not seen for barium hexaaluminate phase II. In the latter case, BaAl_2O_4 and a barium aluminium oxynitride, with a structure similar to barium hexaaluminate phase I, are determined as secondary phases. Thus a solid solution exists for barium hexaaluminate phase I, in contrast to phase II, as represented in Fig. 2. The solid solution can be in equilibrium with barium hexaaluminate phase II, BaAl_2O_4 , $\alpha\text{-Al}_2\text{O}_3$, or AlN . The $\text{BaAl}_2\text{O}_4\text{-Al}_2\text{O}_3$ part of the phase diagram corresponds with the literature (18). The general problems concerning the determination of the exact composition of the barium hexaaluminates have been men-

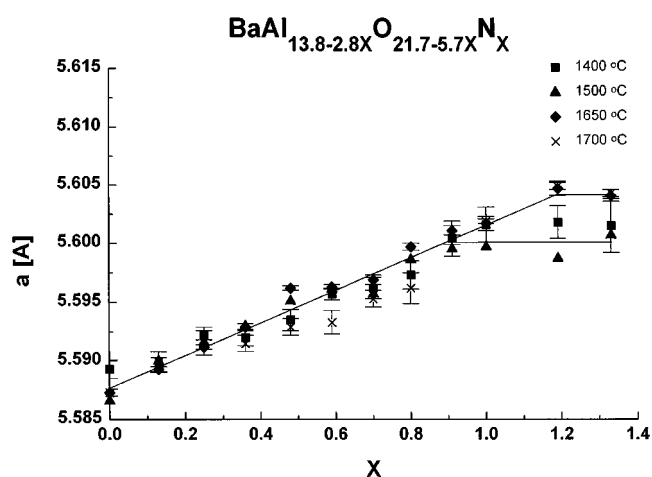


FIG. 3. The a axis as function of the nitrogen content and the firing temperature.

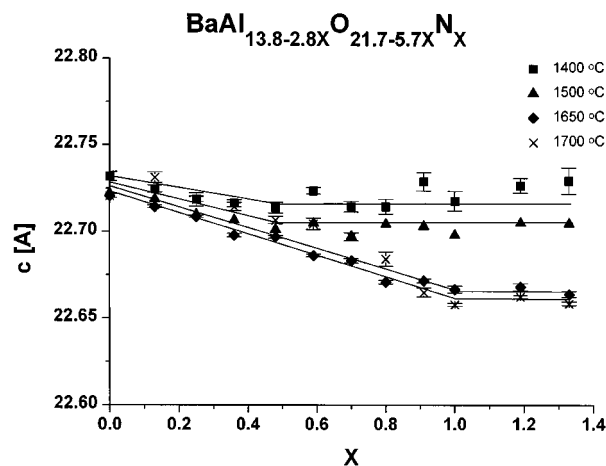


FIG. 4. The c axis as function of the nitrogen content and the firing temperature.

tioned before (19–21). We observed the same problem: in our work, $\text{BaAl}_{13.8}\text{O}_{21.7}$ is assumed as the composition for barium hexaaluminate phase I (19), but sometimes we have determined $\alpha\text{-Al}_2\text{O}_3$ as a secondary phase in a mixture with this nominal composition. Additional investigation showed us that barium hexaaluminate phase I with the composition $\text{BaAl}_{13.2}\text{O}_{20.8}$ is single phase.

In our experiments we did not observe AlON , which according to Willems (23) should be present at temperatures above 1640°C . However, the inaccuracy of the temperature measurements is critical ($\pm 10^\circ\text{C}$) because the firing temperature used (1650°C) is slightly higher than the temperature (1640°C) above which AlON exists.

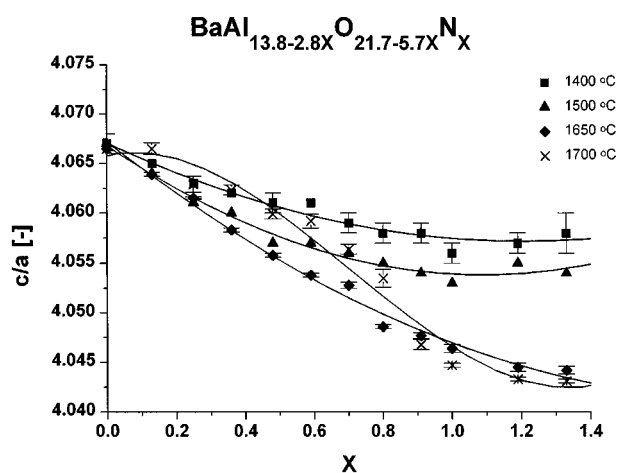


FIG. 5. The c/a ratio as function of the nitrogen content and the firing temperature.

Moving along the solid solution line, as the N/O ratio changes, simultaneously the Ba/Al ratio changes. These ratios are represented by x in the general formula $\text{BaAl}_{13.8-2.8x}\text{O}_{21.7-5.7x}\text{N}_x$ and are used in Figs. 3 to 5. As clear from Figs. 3 and 4, both the a and the c axes are dependent on x . In contrast to what is generally observed, this dependence is different for the a axis compared to the c axis: the a -axis increases with increasing x , while the c axis decreases. This unusual dependence of the unit cell dimensions on the chemical composition is also mentioned for aluminium-oxynitrides with the β -alumina-(Na (13)) or the magnetoplumbite-type structure (L_n (7)), as well as for magnesium aluminates with the β -alumina-(Ba (3)) or the magnetoplumbite-type structure (L_n (25, 26)).

According to Wang *et al.* (7) and Harata *et al.* (13), the increase of the a axis with increasing x is due to the substitution of N^{3-} (with a larger ionic radius $r = 1.7 \text{ \AA}$ (13)), for O^{2-} ($r = 1.4 \text{ \AA}$ (13)). The increase of the a axis is also observed for $\text{BaMgAl}_{10}\text{O}_{17}$ ($a = 5.62 \text{ \AA}$, JCPDS 26-163) with respect to barium hexaaluminate phase I due to the substitution of Mg^{2+} (with a larger ionic radius $r = 0.585 \text{ \AA}$ (27)), for Al^{3+} ($r = 0.39 \text{ \AA}$ (27)). The increase of the a axis is larger for Mg^{2+} substitution in barium hexaaluminate phase I than for N^{3-} substitution, as expected from the ionic radii ratio ($r_{\text{N}^{3-}}/r_{\text{O}^{2-}} \approx 1.2$ and $r_{\text{Mg}^{2+}}/r_{\text{Al}^{3+}} \approx 1.5$). The increase of the a axis and the larger influence of Mg^{2+} versus N^{3-} substitution are also reported for the spinel phase $\gamma\text{-Al}_2\text{O}_3$ ($\text{Al}_{8/3}\square_{1/3}\text{O}_4$) substituted with Mg^{2+} and/or N^{3-} (28). Even more important is the fact that the observed decrease of the c axis in the $\text{N}^{3-}/\text{O}^{2-}$ stabilized barium β -alumina with respect to barium hexaaluminate phase I is also observed in the $\text{Mg}^{2+}/\text{Al}^{3+}$ -stabilized barium β -alumina (see Table 1 and JCPDS 26-163).

To find an explanation for the decrease of the c axis with substitution of N^{3-} or Mg^{2+} , it is necessary to consider what might influence this dimension. The size of the c axis is determined by the intermediate layer thickness (M_{12k}) and by the spinel block thickness (S_{12k}) as follows: $c = 2 \times (M_{12k} + S_{12k})$ (29). As is depicted in Fig. 6, M_{12k} is defined as the distance between O(2) ions at the $12k$ site through the intermediate layer and S_{12k} as the inter-O(2) distance across the spinel block. The intermediate layer is filled with large metal ions (e.g., Ba^{2+}) and O^{2-} ions, while the spinel block is occupied by Al^{3+} and O^{2-} ions. In the following discussion three effects influencing the size of the c axis will be mentioned.

Intermediate Layer Thickness

It is pointed out by Iyi *et al.* (29) that the intermediate layer thickness M_{12k} decreases with increasing metal ion population in this layer. This phenomenon is also found for

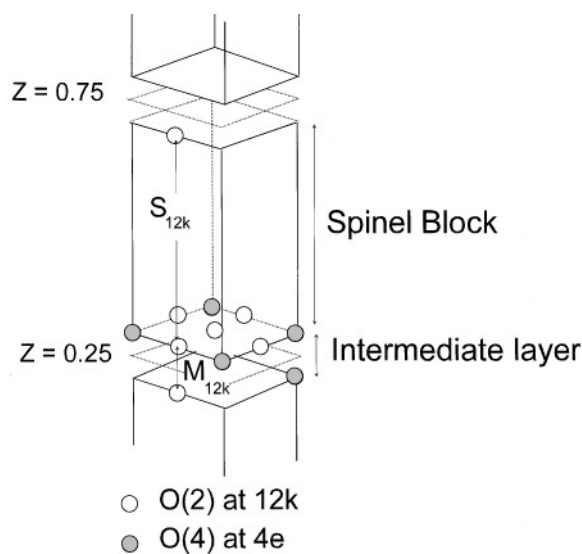


FIG. 6. Simplified hexaaluminate structure, showing the thickness of the intermediate layer M_{12k} and of the spinel block S_{12k} . Open circles represent O(2) at the $12k$ site and shaded circles O(4) at the $4e$ site.

the barium aluminium-oxynitrides, and it has been reported for various other materials with the β -alumina-type structure (29–36). The decrease of the intermediate layer thickness can be explained as follows (29): due to the increasing number of metal ions in the intermediate layer, the charge of this layer becomes more positive. As a result, the negatively charged O(2) ions at the $12k$ site adjacent to the intermediate layer migrate toward the more positively charged layer. Because M_{12k} is defined as the distance between the O(2) ions above and below the intermediate layer, the effect is a decrease of the intermediate layer thickness. According to Iyi *et al.* (29) this decrease is about 0.06 \AA for $\text{BaMgAl}_{10}\text{O}_{17}$ with respect to barium hexaaluminate phase I. It is assumed that this value is comparable to the decrease of the intermediate layer thickness of $\text{BaAl}_{11}\text{O}_{16}\text{N}$ compared to barium hexaaluminate phase I, because the increase of Ba^{2+} ions in the intermediate layer is nearly equivalent.

Because Iyi *et al.* (29) reported the thickness of the intermediate layer (M_{12k}) of barium hexaaluminate phase I and $\text{BaMgAl}_{10}\text{O}_{17}$, it is possible to calculate the spinel block thickness from the lattice parameter c . With $c = 22.7207 \text{ \AA}$ (Table 1) and $M_{12k} \approx 4.68 \text{ \AA}$ (29) the spinel block thickness for barium hexaaluminate phase I is about 6.68 \AA . Assuming that the thickness of the intermediate layer in $\text{BaAl}_{11}\text{O}_{16}\text{N}$ is equal to that in $\text{BaMgAl}_{10}\text{O}_{17}$ ($M_{12k} \approx 4.62 \text{ \AA}$ (29)), it is possible to calculate the spinel block thickness of $\text{BaAl}_{11}\text{O}_{16}\text{N}$. With $c = 22.6579 \text{ \AA}$ (Table 1) the spinel block thickness, S_{12k} , of $\text{BaAl}_{11}\text{O}_{16}\text{N}$ is about 6.71 \AA , which is slightly increased (0.03 \AA) with respect to barium hexaaluminate phase I.

Spinel Block Thickness

1. Analogous to the increase of the size of the a axis, it is expected that the substitution of O^{2-} by N^{3-} as such will result in an increase of S_{12k} .

2. It is reported by Iyi *et al.* (29) that the spinel block thickness S_{12k} decreases with decreasing amount of Al^{3+} vacancies within the spinel block. These vacancies are part of the Frenkel-type defect that is observed in various β -alumina materials (19, 37, 38). This defect results in a shift of some Al^{3+} ions from the spinel block to the intermediate layer, leaving Al^{3+} vacancies in the spinel block and creating interstitial Al^{3+} near the intermediate layer, as is shown in Fig. 7. Simultaneously, interstitial O^{2-} is present in the intermediate layer, replacing Ba^{2+} in one of every four intermediate layers (38). These oxygen ions are necessary to maintain the charge balance in the barium hexaaluminate phase I structure (38). As a result of the Mg^{2+} substitution, no Frenkel-type defect is necessary for maintaining the charge balance in the β -alumina structure (39) and the same is assumed to be true for the N^{3-} substitution.

With an increase of the spinel block thickness of 0.03 \AA for the $BaAl_{11}O_{16}N$ material with respect to barium hexaaluminate phase I, the effect of the difference in ionic radius (N^{3-} versus O^{2-}) is larger than the effect of the decrease of the concentration in Frenkel defects.

As is clear from Figs. 3 and 4, the dependence of the unit cell dimensions on the chemical composition is influenced by the firing temperature. This is ascribed to the fact that the amount of nitrogen that can be incorporated in the barium hexaaluminates is dependent on the temperature. As has been mentioned already, the size effect of the a axis is specified fully by the nitrogen content. This means that the size of the a axis does not change when the maximum

amount of nitrogen is incorporated. Thus according to Fig. 3 the maximum amount of nitrogen incorporated at 1400 and 1500°C is $x \approx 0.9$ ($BaAl_{11.28}O_{16.57}N_{0.9}$), but for higher firing temperatures (1650 and 1700°C) it is $x \approx 1.2$ ($BaAl_{10.44}O_{14.86}N_{1.2}$). These compositions cannot be deduced from Fig. 4, because the size of the c axis is influenced also by the barium content. For both temperature ranges (1400–1500°C and 1650–1700°C) the turning points in Fig. 4 (c axis) are lower than in Fig. 3 (a axis). This means that above these turning points the size effects on the intermediate layer (M_{12k}) and/or the spinel block thickness (S_{12k}) are changed. What happens precisely above these turning points will be investigated in the near future.

The c/a ratio as a function of the chemical composition and the firing temperature (Fig. 5) is clearly influenced by the different mechanisms that are determining the size of the a and c axis. The decrease of the c/a ratio is larger at high firing temperatures (1650–1700°C) for compositions with a relatively high x value. This is caused by a further increase of the a axis and a further decrease of the c axis with increasing x value at high temperatures (see Figs. 3 and 4). The turning points in Fig. 5 are in between those of Figs. 3 and 4, as a consequence of the mixed influence of the a and the c axis.

For barium aluminium-oxynitrides it is clear that these materials have the β -alumina-type structure, both by the presence of the solid solution with barium hexaaluminate phase I and by the fact that the c/a ratio is above 4. But for materials with the magnetoplumbite-type structure it is not clear if this structure type remains the same after nitrogen substitution. At this moment, we are investigating (40) the existence of oxynitrides with the magnetoplumbite structure, similar to the lanthanide magnetoplumbite-type materials (7). Another possibility that will be examined is the existence of oxynitride materials with the β -alumina-type structure that are derived from oxide magnetoplumbite-type materials, in a similar way as that determined for magnesium stabilized materials (14).

CONCLUSIONS

The phase relations in the $BaO-Al_2O_3-AlN$ system have been investigated at room temperature with powder X-ray diffraction at several firing temperatures. It has been shown that a new β -alumina (space group $P6_3/mmc$) can be synthesized: a barium aluminium-oxynitride. The solid solution is formed with barium hexaaluminate phase I ($BaAl_{13.8}O_{21.7}$) and its extent is dependent on the firing temperature. At 1400–1500°C this compound has the boundary composition of approximately $BaAl_{11.28}O_{16.57}N_{0.9}$ and at 1650–1700°C it has the boundary composition of approximately $BaAl_{10.44}O_{14.86}N_{1.2}$.

The unit cell dimensions vary with the chemical composition depending on the firing temperature. Starting from

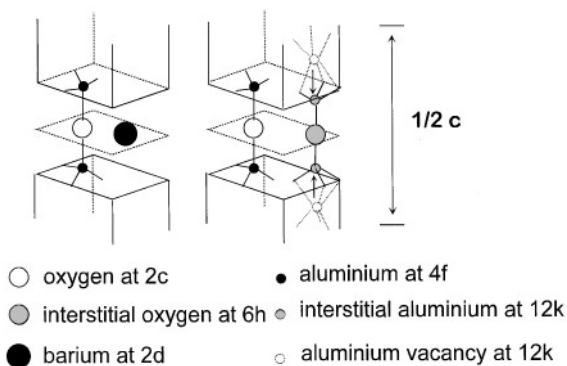


FIG. 7. Two kinds of half of the unit cell assumed to constitute barium hexaaluminate phase I. The left half of the unit cell containing barium and oxygen ions in the intermediate layer. The right half of the unit cell containing interstitial aluminium and oxygen ions replacing the barium ion. The arrow indicates the shift of the aluminium ions due to the Frenkel defect mechanism.

barium hexaaluminate phase I, the size of the *a* axis from the compounds along the solid solution line increases with increasing nitrogen content. This can be ascribed to the replacement of an O²⁻ ion by a larger N³⁻ ion. On the other hand, the size of the *c* axis from the compounds along the solid solution line decreases simultaneously with the increase of the *a* axis. The *c* axis can be considered as composed of two parts: the intermediate layer and the spinel block. The decrease of the *c* axis can be ascribed to three simultaneously occurring effects:

1. the intermediate layer thickness should decrease owing to an increase in the concentration of barium ions in this layer when O²⁻ is substituted by N³⁻;
2. an increase in spinel block thickness is expected (similar to the *a* axis) when O²⁻ is replaced by N³⁻;
3. the spinel block thickness should decrease as a consequence of a decrease of the number of Frenkel-type defects induced by the N³⁻ to O²⁻ replacement.

ACKNOWLEDGMENTS

The authors acknowledge Philips Lighting, who sponsored this study, and R. P. A. Timmermans, B. P. Rijpers, M. S. A. Eekhof, and J. G. H. Groenhagen for helping with the sample preparation and X-ray diffraction measurements.

REFERENCES

1. R. Collongues, D. Gourier, A. Kahn-Harari, A. M. Lejus, J. Théry, and D. Vivien, *Ann. Rev. Mater. Sci.* **20**, 51 (1990).
2. R. Collongues, D. Gourier, A. Kahn, J. P. Boilot, P. Colomban, and A. Wicker, *J. Phys. Chem. Solids* **45** (10), 981 (1984).
3. J. M. P. J. Versteegen and A. L. N. Stevels, *J. Lumin.* **9**, 406 (1974).
4. G. W. Schäfer, A. Van Zyl, and W. Weppner, *Solid State Ionics* **40/41**, 154 (1990).
5. B. C. Tofield, "Intercalation Chemistry" (M.S. Whittingham and A. J. Jacobson, Eds.), p. 181. Academic Press, New York, 1982.
6. J. M. P. J. Versteegen, J. L. Sommerdijk, and J. G. Verriet, *J. Lumin.* **6**, 425 (1973).
7. X. H. Wang, A. M. Lejus, D. Vivien, and R. Collongues, *Mater. Res. Bull.* **23**, 43 (1987).
8. W. Y. Sun, T. S. Yen, and T. Y. Tien, *J. Solid State Chem.* **95**, 424 (1991).
9. W. Y. Sun and T. S. Yen, *Mater. Lett.* **8** (5), 145 (1989).
10. W. Y. Sun and T. S. Yen, *Sci. China, Ser. A* **34** (1), 105 (1991).
11. Y. F. Yu Yao and J. T. Kummer, *J. Inorg. Nucl. Chem.* **29**, 2453 (1967).
12. H. Näfe and M. Steinbrück, *J. Electrochem. Soc.* **141** (10), 2779 (1994).
13. M. Harata, A. Imai, T. Ohta, and S. Sugaike, *Solid State Ionics* **3/4** 409 (1981).
14. A. L. N. Stevels and A. D. M. Schrama-de Pauw, *J. Electrochem. Soc.* **5**, 691 (1976).
15. B. M. J. Smets and J. G. Verlijdsdonk, *Mater. Res. Bull.* **21**, 1305 (1986).
16. S. R. Jansen, H. T. Hintzen, and R. Metselaar, "Proceedings of the Fourth Conference of the European Ceramic Society" (C. Galassi and S. Meriani, Eds.), p. 441. Gruppo editoriale faenze editrice S.p.A., Riccione, 1995.
17. P. P. Budnikov and A. M. Ginstling, "Principles of Solid State Chemistry: Reactions in Solids" (P. P. Budnikov and A.M. Ginstling, Eds.), p. 328. MacLaren and Sons LTD, London, 1968.
18. S. Kimura, E. Bannai, and I. Shindo, *Mater. Res. Bull.* **17**, 209 (1982).
19. N. Iyi, Z. Inoue, S. Takekawa, and S. Kimura, *J. Solid State Chem.* **52**, 66 (1984).
20. G. Groppi, F. Assandri, M. Bellotto, C. Cristiani, and P. Forzatti, *J. Solid State Chem.* **114**, 326 (1995).
21. M. K. Cinibulk, *J. Mater. Sci. Lett.* **14**, 651 (1995).
22. S. R. Jansen, H. T. Hintzen, and R. Metselaar, *J. Mater. Sci. Lett.* **15**, 794 (1996).
23. H. X. Willems, "Preparation and Properties of Translucent Gamma-Aluminium Oxynitride." Ph.D. thesis, Eindhoven University of Technology, The Netherlands, 1992.
24. S. R. Jansen, K. S. Knight, H. T. Hintzen, and R. Metselaar, to be published.
25. N. Iyi, Z. Inoue, S. Takekawa, and S. Kimura, *J. Solid State Chem.* **54**, 70 (1984).
26. D. Saber and A.M. Lejus, *Mater. Res. Bull.* **16**, 1325 (1981).
27. H. St. C. O'Neill and A. Navrotsky, *Am. Mineral.* **68**, 181 (1983).
28. A. Granon, P. Goeuriot, F. Thevenot, J. Guyader, P. L'Haridon, and Y. Laurent, *J. Eur. Ceram. Soc.* **13**, 365 (1994).
29. N. Iyi, S. Takekawa, and S. Kimura, *J. Solid State Chem.* **83**, 8 (1989).
30. J. M. Newsam and B. C. Tofield, *Solid State Ionics* **5**, 59 (1981).
31. J. P. Boilot, G. Collin, Ph. Colomban, and R. Comès, *Solid State Ionics* **5**, 157 (1981).
32. F. Harbach, *J. Mater. Sci.* **18**, 2437 (1983).
33. G. J. Dudley and B. C. H. Steel, *J. Mater. Sci.* **13**, 1267 (1978).
34. M. P. Anderson, L. M. Foster, and S. J. La Place, *Solid State Ionics* **5**, 211 (1981).
35. M. P. Anderson and L. M. Foster, *Solid State Ionics* **5**, 219 (1981).
36. T. Tsurumi, H. Ikawa, K. Urabe, and S. Udagawa, *Yogyo Kyokai Shi* **91**, 553 (1983).
37. W. L. Roth, F. Reidinger, and S. LaPlaca, "Superionic Conductors" (W. L. Roth, Ed.), p. 223. Plenum, New York, 1976.
38. F. P. F. Van Berkel, H. W. Zandbergen, G. C. Verschoor, and D. J. W. IJdo, *Acta Crystallogr. C* **40**, 1124 (1984).
39. G. Collin, R. Comes, J. P. Boilot, and P. Colomban, *Solid State Ionics* **1**, 59 (1980).
40. S. R. Jansen, H. T. Hintzen, and R. Metselaar, to be published.